Comput Mech (2013) 52:151–159
DOI 10.1007/s00466-012-0803-x

ORIGINAL PAPER

Computational analysis of temperature rises in microstructures of HMX-Estane PBXs

Ananda Barua · Min Zhou

Received: 10 May 2012 / Accepted: 23 September 2012 / Published online: 9 October 2012

Abstract The thermomechanical response of HMX/Estane, a polymer-bonded explosive (PBX) is analyzed for initial temperatures between 210 and 300 K. The main objective of this analysis is to gain a better understanding of the concepts that lead to deformation and heating of energetic composites as they undergo mechanical and thermal processes subsequent to impact. A recently developed cohesive finite element method (CFEM) framework is used to study the microstructure-level response of PBX. The CFEM framework allows the contributions of individual constituents, fracture and frictional contact along failed crack surfaces to heating to be tracked and analyzed. Digitized micrographs of actual PBX materials are used. The issues studied include large deformation, thermomechanical coupling, failure in the forms of microcracks in both bulk constituents and along grain/matrix interfaces, and frictional heating. The focus is on the correlation between grain-level failure mechanisms and overall temperature rise in the PBX. The results are used to establish microstructure-response relations that can be used in the design of energetic composites.

Keywords Thermomechanical response · Cohesive framework · Contact · Polymer-bonded explosives · Microstructure modeling

Communicated by M. Zhou.

A. Barua (✉) · M. Zhou
Woodruff School of Mechanical Engineering, Georgia Institute of Technology, 801 Ferst Drive N.W., Atlanta, GA 30332, USA
e-mail: abarua@gatech.edu

M. Zhou
School of Materials Science and Engineering, Georgia Institute of Technology, 801 Ferst Drive N.W., Atlanta, GA 30332, USA
e-mail: min.zhou@gatech.edu

1 Introduction

Polymer bonded explosives belong to a class of energetic materials consisting of a heterogeneous mixture of explosive crystals (such as HMX and RDX) and polymeric binder (e.g., HTPB and estane). The content of explosives in the composite can vary from 60 to 95 % by mass. They are used in various applications such as solid rocket propellants and insensitive munitions (e.g. HMX/estane). The next generation munitions are expected to experience stresses on the order of several GPa upon impact. The heterogeneous nature of the microstructure renders the impact response of PBXs non-scalable. At the grain level, the initiation of reaction is controlled by processes occurring within the crystals, in the polymer binder and along the interfaces between the two. Propagation of reaction depends on microstructural parameters such as grain morphology, packing density and defects. Current design paradigms focus on a high level of empiricism, which is time consuming and costly.

When PBXs are subject to impact loading, various grain-level mechanisms are activated, causing localized energy dissipation in the microstructure. The nature of energy localization is highly dependent on the loading density and time after impact. The detonation of energetic materials is known to initiate in hot-spots [1] which can be identified as local high temperature regions having a sufficient size and temperature to cause chemical reactions. Both chemical and mechanical processes contribute to the initiation of reaction. The phase transformation and chemical reactions leading to combustion of PBXs are well established [2,3]. However, the mechanisms related to hot-spot formation are not well understood, primarily due to the lack of experimental data in this regard.

The addition of the polymeric binder changes the response of PBXs. Several experimental studies have focused the behavior at different strain rates (see e.g., Gray III et al.

[4], Govier et al. [5]). Split Hopkinson pressure bar experiments show various degrees of dependence of the stress-strain responses of different PBXs on initial temperature and strain rate [6]. This, combined with post-mortem analyses of specimens, show that PBXs are likely to fail by cleavage of the crystals at temperatures below the glass transition temperature of the binder and by debonding along grain-matrix interfaces at higher temperatures [5]. The results clearly indicate viscoelasticity of the binder and microstructural fracture as important deformation and failure mechanisms that must be accounted for in mesoscale models. Quantitative information about the stress and displacement fields at the microstructural level can be obtained by using digital image correlation [7], allowing calibration of phenomenological interface separation laws for the different types of surface pairs in the composite.

Numerical analyses are widely used to gain insight into the complex grain-level responses of particulate composites under dynamic loading. Eulerian-formulation-based approaches have been used to study the effect of viscosity on hot-spot formation (see, e.g., Benson and Conley [1]), compaction wave profiles (Baer [8], Trott et al. [9]) and hot-spot formation due to pore collapse in PBX (Menikoff [10]). In particular, Trott et al. [9] found a good correlation between calculated and measured wave profiles. The results suggest that the complex mechanisms leading to energy release at the mesoscale can be delineated if accurate material models and realistic microstructures are used.

So far, Eulerian simulations have not attempted to capture interfacial debonding and interactions between binder and gains and fracture surfaces inside grains. These failure mechanisms cause overall loss of strength and lead to frictional dissipation at fractured surfaces. Experiments performed at low impact velocities on the order of $50\,\mathrm{ms}^{-1}$ showed decreasing delays in detonation [11] as projectile velocity is increased. The result suggests that fracture and frictional dissipation play a significant role in temperature rises in the microstructure. Lagrangian formulations can more effectively track interfacial movements (Ortiz et al. [12]). Such methods can account for fracture, interfacial interactions between grains and binder and between grains. Previous studies using Lagrangian approaches (see, e.g., Banerjee et al. [13], Wu et al. [14]) suggest that the effect of grain/binder debonding weakens the composite and influences other dissipation mechanisms.

In the current study, a CFEM-based framework [15–18] is used, accounting for microstructure and thermal–mechanical processes such as shear banding, interfacial debonding and fracture of grains. Here, cohesive elements are embedded throughout the microstructure, along all elements boundaries, as in [19]. This approach allows arbitrary fracture paths and patterns inside each phase and along the interfaces between the phases to be resolved. Contact and friction between failed crack surfaces are accounted for, allowing heating due to interfacial sliding to be analyzed along with heating due to bulk constitutive inelasticity.

We evaluate the effects of changes in the initial temperature on the impact response of a HMX/estane PBX. Fracture mechanisms considered include crack initiation, growth and coalescence inside bulk constituents and along interfaces between the HMX and estane binder. Initial temperatures between 210 and 300 K are considered, covering the glass transition temperature T_g (243 K) of the binder. The objective is to obtain a correlation between the grain-level failure mechanisms and macroscopic behavior of the PBX over the temperature regime. Ultimately, the goal is to develop predictive models for the design of better and more efficient energetic composites.

2 Microstructure-level model

The micrograph shown in Fig. 1 is obtained from [20]. This image is used to generate the cohesive finite element model shown in Fig. 1b.

The finite element discretization is based on linear-displacement triangular elements arranged in a 'crossed-triangle' quadrilateral pattern. Cohesive elements are embedded throughout the microstructure, along all elements boundaries, as in [15–18,21]. This approach allows arbitrary fracture paths and patterns inside each phase and along the interfaces between the phases to be resolved. This form of CFEM obviates the need for separate criteria for fracture initiation and propagation. Another way to look at it is that the cohesive relation serves as the fracture initiation and propagation criteria. However, this approach does require the model to satisfy limitations on mesh density and cohesive stiffness (Tomar et al. [22]). This issued is addressed by the use of a sufficiently large initial cohesive stiffness ($\eta_0 = 0.001$) and a finite element size of $30\,\mu\mathrm{m}$ [15].

The cohesive elements follow a traction-separation law relating the traction on the cohesive surface pair and the interfacial separation. The bilinear traction-separation law developed by Zhai and Zhou [21] is used here. This relation can be regarded as a generalized version of those given by Tvergaard and Hutchinson [23] and Ortiz and Pandolfi [12]. The work done in fully separating a pair of surfaces is set to be equal to the respective critical energy release rate $\mathscr{G}$ of the particular fracture surface pair (within a HMX granule, inside the ESTANE binder, and along a HMX-Estane interface). Experimental values of $\mathscr{G}$, when available, are used to guide the determination of the cohesive parameters. The values of $\mathscr{G}$ for the binder and interface are taken from Tan et al. [7].

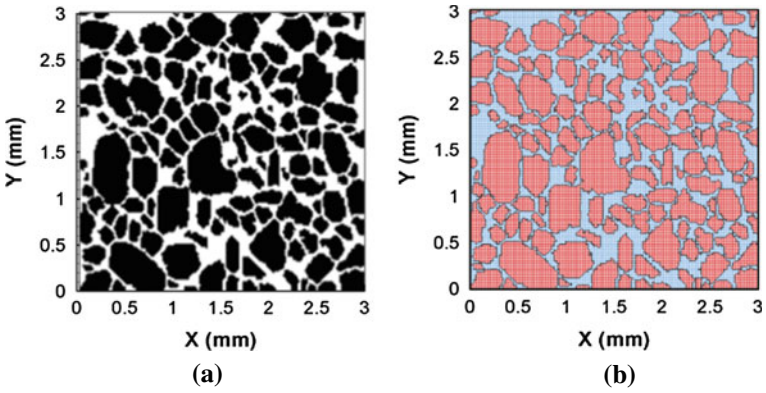

Fig. 1 **a** Image of a PBX microstructure consisting of energetic crystals (grains) and a polymer binder from [20], **b** CFEM microstructural model of the digitized image, the grain volume fraction is 0.69

Under compression, penalty traction is used to apply sufficient normal traction on the corresponding node pairs to strongly discourage interpenetration of cohesive surfaces.

Failure of cohesive elements results in creation of surfaces. In order to prevent interpenetration, a contact algorithm similar to that in Camacho and Ortiz [24] is developed and used. This algorithm works in two steps, the first step involves the detection of potential contact surfaces and the second step involves the application of penalty forces to prevent interpenetration. A normal penalty force is applied to correct the overlap of elements. The Coulomb friction law is used to determine the frictional force between a contacting surface pair and, in turn, the tangential component of the nodal force vector. Frictional dissipation is calculated based on relative interfacial slip and frictional force and is added to the thermal energy change for the respective nodes.

3 Microstructural constituents

The binder in the microstructure analyzed is a commercially available polymer known as ESATNE 5703 which is used in explosive PBX 9501. It has a glass transition temperature (T_g) of 243 K. This material is viscoelastic, with properties sensitive to both strain rate and temperature. The composition and mechanical properties of plasticized estane can be found in [25].

HMX (octahydro-1,3,5,7-tetranitro-1,3,5,7-tetrazocine) granules are the explosive content. It is an anisotropic crystal and is brittle at ambient pressures and therefore undergoes very little plastic deformation. Hence, dissipation associated with dislocation motion and plastic deformation is small compared with the energy spent on fracture development and subsequent frictional dissipation along crack faces. Since this study focuses on non-shock conditions, an elastic constitutive model for HMX is justified. A hyperelastic constitutive formulation is used for HMX, the material properties for which are obtained from [9].

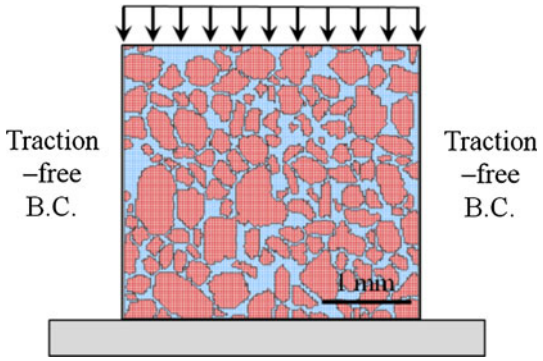

Fig. 2 Loading configuration of an unconfined specimen with traction-free boundary condition on the lateral sides

Damage accumulation in the crystals is accounted for via cohesive surfaces embedded throughout the microstructure, as described in the previous section.

4 Loading configuration

A 3-mm square microstructural region initially stress-free and at rest is analyzed. The traction-free boundary condition (Fig. 2) for the lateral sides allows conditions of nominally uniaxial stress (unconfined, low stress triaxiality) to be simulated. This is a 2D model and the conditions of plane-strain prevail. The velocity boundary condition at the top surface and the fixed displacement boundary condition at the bottom surface allow prescribed deformation rates to be imposed.

5 Model calibration

The overall response of PBX includes contributions from both the deformation of bulk constituents and the debonding at grain-matrix interfaces. Figure 3 shows a comparison between measured and calculated stress-strain responses of PBX 9501 for three initial temperatures from 233 to 290 K and a strain rate of $\dot{\varepsilon} = 2{,}500\,\mathrm{s}^{-1}$. The calculations are

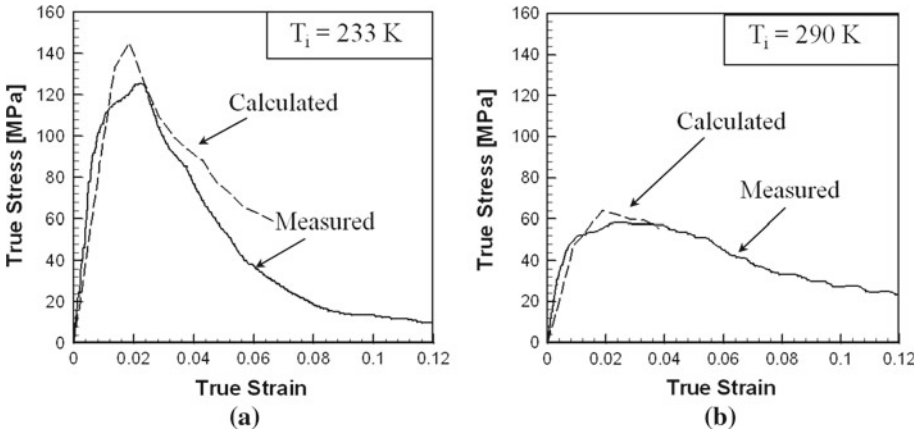

Fig. 3 Calculated and measured stress-strain curves for PBX-9501 (experiments by Gray et al. [4], strain rate $\varepsilon = 2{,}500\,\mathrm{s}^{-1}$, grain fraction $\eta = 0.69$)

based on the microstructure shown in Fig. 1. The calculated and measured stress-strain profiles show good correlation. Note that at the lower temperature of 233 K, the calculation over-predicts the stress in the softening portion of the response. One possible reason is that at low temperatures, the brittle behavior of the binder causes the response to be more sensitive to the microstructural heterogeneity. At the higher temperature (293 K), the binder behaves in a more ductile manner and the response is less dependent on the microstructure. The above comparisons between calculated and experimental results serve as a justification for the bulk constitutive and fracture parameters used in the present analyses.

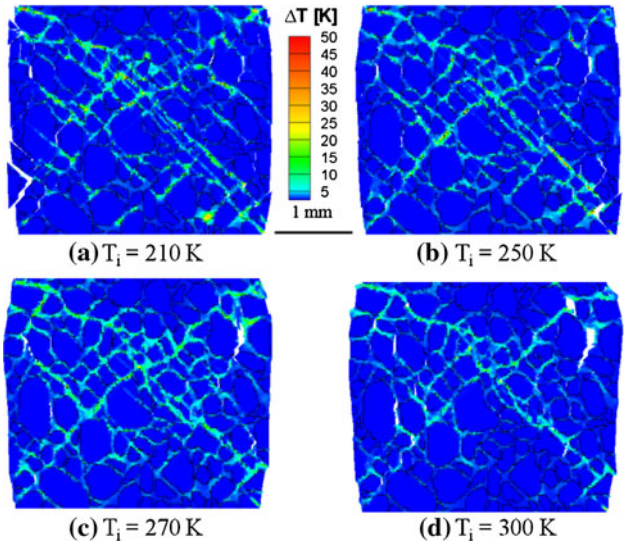

Fig. 4 Distribution of temperature increase in the microstructure at $t = 4.0\,\mu\mathrm{m}$ ($\varepsilon = 5.83\,\%$) for four different cases: **a** $\mathrm{T_i} = 210\,\mathrm{K}$, **b** 250 K, **c** 270 K, and **d** 300 K (the nominal strain rate is $\dot{\varepsilon} = 16{,}667\,\mathrm{s}^{-1}$)

6 Results and discussions

A systematic analysis is carried out, focusing on the effect of initial temperature. The framework is inert, so the effects of possible phase transitions and chemical reactions are not considered. The imposed boundary velocity at the top surface of the configurations in Fig. 2 is $\mathrm{V_0} = 50\,\mathrm{ms}^{-1}$ (which gives rise to a nominal strain rate of $\dot{\varepsilon} = 16{,}667\,\mathrm{s}^{-1}$) with a linear ramp from zero to $\mathrm{V_0}$ in the first 1 μs of loading. Here, we discuss results at four different initial temperatures (210, 250, 270 and 300 K).

Figure 4 shows the distribution of temperature rise over the initial temperature ($\Delta\mathrm{T} = \mathrm{T} - T_i$) at time $t = 4.0\,\mu\mathrm{s}$ ($\varepsilon = 5.83\,\%$) after the onset of loading for different values of initial temperature. For all calculations, the distribution of temperature is influenced by the microstructural heterogeneity. High temperature rises are localized mainly in bands in the matrix. These high temperature bands extend diagonally across the microstructure, approximately following the direction of maximum shear stresses. The temperature sensitivity of the binder causes different failure mechanisms to be active at different temperature regimes.

At 210 K ($\mathrm{T_i} < \mathrm{T_g}$), the dominant failure mechanism is the fracture of bulk constituents. Cracks develop in the binder and coalesce with transgranular cracks in the grains to form continuous failure paths. The fracture paths run through the grains and binder, resulting in fragmentation of the composite (see Fig. 5). This can be observed at the lateral surfaces of the microstructure in Fig. 5a. At this temperature, the binder is hard and brittle, causing high stresses to be developed. Consequently, the stress-strain profiles show higher peak stresses (Fig. 3). Subsequent loading causes the binder to fail by brittle fracture characterized by a sharp drop in stress. Relative sliding of fractured surfaces results in high frictional dissipation and temperature rises in the microstructure (Fig 5a).

As the initial temperature is increased beyond $\mathrm{T_g}$, the binder increasingly behaves as a soft, viscous material. In early stages of loading, deformation is primarily accommodated by the softer binder, causing heating in the binder and

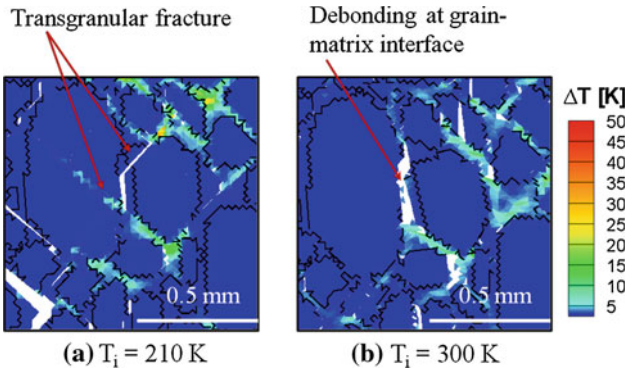

Fig. 5 Close-up view of a region of the microstructure at $t = 4.0$ μm ($\varepsilon = 5.83\,\%$) showing the different failure mechanisms at **a** $T_i = 210$ K and **b** 300 K (the nominal strain rate is $\dot{\varepsilon} = 16{,}667\ s^{-1}$)

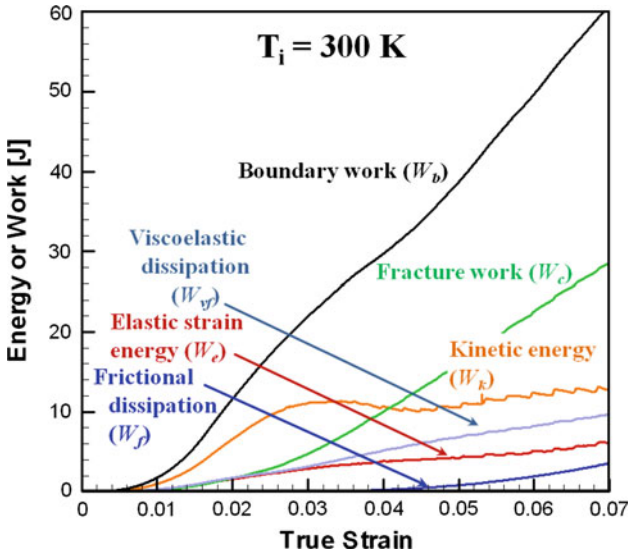

Fig. 6 Evolution of mechanical work and dissipation, $T_i = 300$ K and $\dot{\varepsilon} = 16{,}667\ s^{-1}$

heat conduction into the grains across the grain-binder interface. Initially, higher temperature rises occurs in regions of the binder between neighboring grains carrying high normal and shear stresses. Subsequently, these areas coalesce to form shear bands. It is noted that shear bands in the binder alone typically do not generate sufficient heat to cause melting of the HMX grains.

The soft binder allows relative motion of grains to take place, activating other energy dissipation mechanisms. Debonding along the relatively weak grain-matrix interface is the primary mode of damage (Fig. 5b). Such interfacial debonding has also been experimentally observed in experiments at both low and high strain rates (see, e.g., Rae et al. [26], Siviour et al. [20]). This form of damage reduces the effective modulus of the overall microstructure (Banerjee et al. [13]). At higher levels of nominal strain (>3 %), grain–grain interactions occur.

The locations where grains come into contact with each other are sites of severe stress concentration, crack development and grain–matrix sliding. Crack formation, sliding and the ensuing frictional dissipation cause more intense heating and higher temperatures. Further deformation leads to transgranular fracture of grains. Crack development, grain–matrix debonding and transgranular fracture create more surfaces which may come into contact and slide against one another giving rise to additional frictional dissipation and heating. These processes ultimately lead to more severe heating in the microstructure, resulting in what is known as the hot-spots which can cause ignition of energetic materials [27].

We first consider the case with $T_i = 300$ K and will use it as the basis for comparison. Figure 6 shows the evolution of total mechanical work imparted to the microstructure by the applied load or boundary work (W_b), elastic strain energy (W_e), and kinetic energy (W_k). The three forms of energy dissipation–energy spent on causing fracture or fracture energy (W_c), viscoelastic dissipation (W_{ve}) and frictional dissipation (W_f)—are also shown. Only W_{ve} and W_f contribute to temperature rises in the microstructure. Boundary work (W_b) increases nearly linearly to 60 J as the nominal strain reaches 0.07. Initially, the increase in kinetic energy (W_k) is higher than the increase in elastic strain energy (W_{ve}), indicating that more energy is stored in the specimen as kinetic energy than as elastic strain energy. Beyond a nominal strain of 0.04, the rate of change of W_k decreases and becomes approximately equal to the rate of change of W_f, indicating a gradual decrease in specimen acceleration and the intensification of fracture and heating due to viscoelastic and frictional dissipation. Energy dissipated through fracture increases linearly up to 30 J as the overall strain increases to 0.07. At this value of overall strain, W_c constitutes and W_c (8.6 %). The viscoelastic dissipation (W_{ve}) is primarily associated with the shear deformation of the binder and accounts for ∼15.9 % of the overall boundary input (W_b). In contrast, elastic strain energy (W_e) accounts for ∼10.2 %.

The evolution of elastic strain energy, viscoelastic dissipation and frictional dissipation with overall strain for four initial temperatures between 210 and 300 K are shown in Fig. 7a–c. The elastic strain energy is higher at lower initial temperatures, indicating the effect of higher elastic modulus of the binder at lower temperatures. In contrast, viscoelastic dissipation in the binder does not show a clear trend with the variation of initial temperature. Specifically, W_{ve} is low at both $T_i = 210$–300 K and is highest at an intermediate temperature of 270 K. At 210 K ($<T_g$), the binder is relatively brittle, consequently, viscous dissipation is insignificant. At $T_i > T_g$, the softer binder absorbs most of the input energy and accommodates most of the imposed deformation. Increasing the initial temperature beyond T_g causes higher viscoelastic dissipation. Between 25 and 270 K, the binder

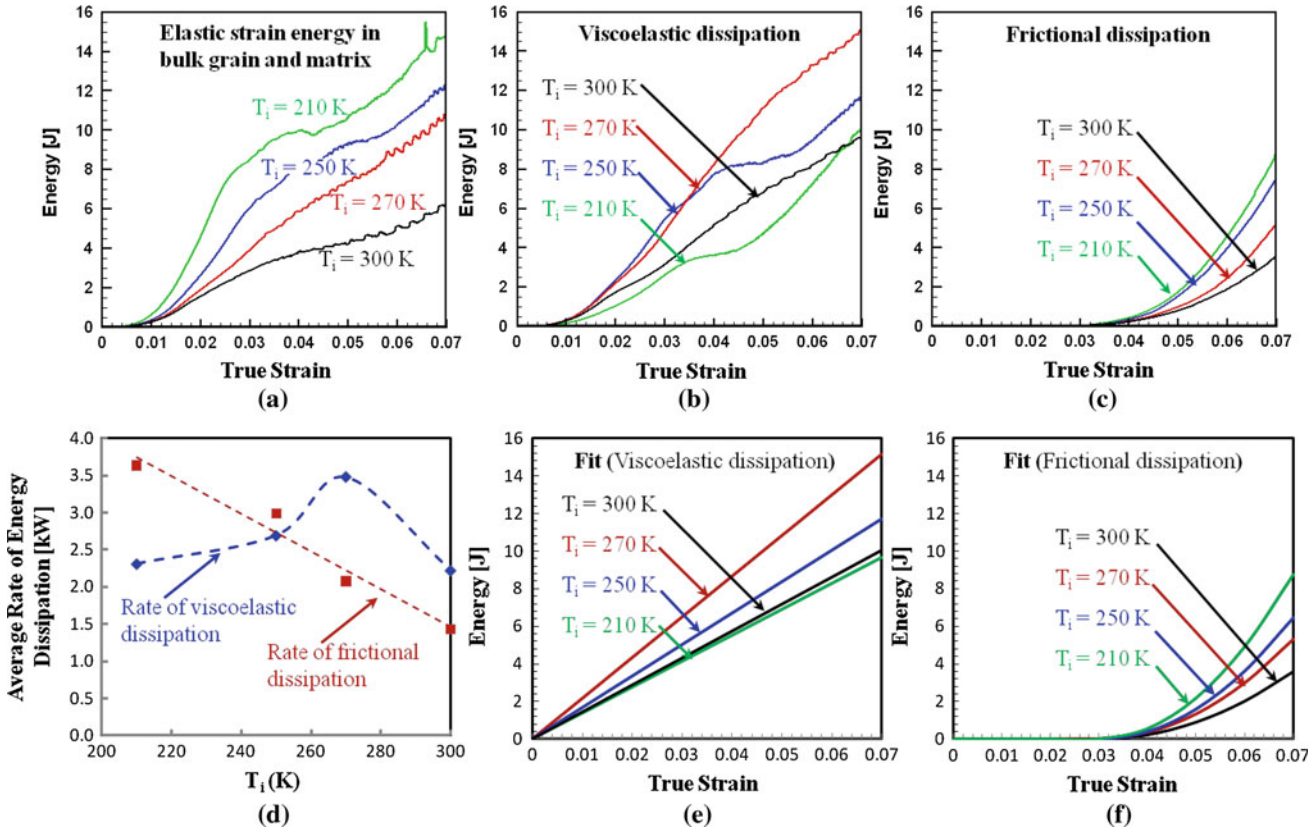

Fig. 7 Evolution of elastic strain energy and dissipation with over strain ($T_i = 210$–$300\,K$ and $\dot{\varepsilon} = 16{,}667\,s^{-1}$), **a** elastic strain energy, **b** viscoelastic dissipation, **c** frictional dissipation, **d** average dissipation rates, **e** fit for viscoelastic dissipation, and **f** fit for frictional dissipation

is hard enough for high stresses to be developed, causing higher viscous dissipation. At 250 K, the rate of viscous dissipation decreases beyond a nominal strain of 4 %, owing to increased fracture in the microstructure. At a higher temperature of 300 K, the binder is soft enough to prevent high stresses from being developed, causing viscous dissipation in the binder to decrease.

Viscoelastic dissipation in the binder is the primary dissipation mechanism in early stages of the deformation. Accordingly, temperature increase occurs primarily in the binder. Although the binder is typically inert, a portion of the thermal energy is conducted into the grains through the grain-matrix interface. Thus, part of the temperature increase in the grains is due to viscous dissipation in the binder.

Figure 7c shows the energy dissipated due to frictional heating in bulk grains and matrix. Clearly, higher overall stresses and more extensive fracture at lower initial temperatures lead to higher levels of frictional dissipation. Since no fracture occurs in early stages of loading, frictional dissipation remains zero for strains up to 3 %. Beyond this strain, frictional dissipation initiates in both bulk phases and along the grain-matrix interfaces.

The contributions of viscoelastic and frictional dissipations to temperature rises in the microstructure vary with initial temperature. Quantifying the dissipations provides insight into the heating mechanisms and their temperature- and time-dependence. Figure 7d plots the rates of viscoelastic and frictional dissipations at different values of initial temperature. The rates are averaged over the duration of deformation up to 0.07. It can be seen that the rate of viscoelastic dissipation is low ($\sim$ 2.3 kW) at both ends of the temperature range (210–300 K) and reaches a maximum value of around 3.48 kW at the intermediate temperature of $T_i = 270\,K$. Deformation and viscoelastic dissipation in the binder are lower at low temperatures (e.g., 210 K) because the brittle nature of the binder enhance failure and frictional dissipation in both phases. While at high temperatures (e.g., 300 K), lower overall stresses translate into lower viscoelastic dissipation. For each initial temperature, viscoelastic dissipation (W_{ve}) increases essentially linearly with time (Fig. 8b). In such cases, the rate of viscous dissipation $W'_{ve}(t)$ can be assumed to be a constant which dependents only on T_i, i.e.,

$$W'_{ve}(t) = C(T_i); \quad t \geq 0. \tag{6.1}$$

where $C(T_i)$ is the average rate of viscous dissipation as shown in Fig. 8d. Thus, the viscous dissipation can be obtained as a function of time by simply integrating Eq. (6.1) as,

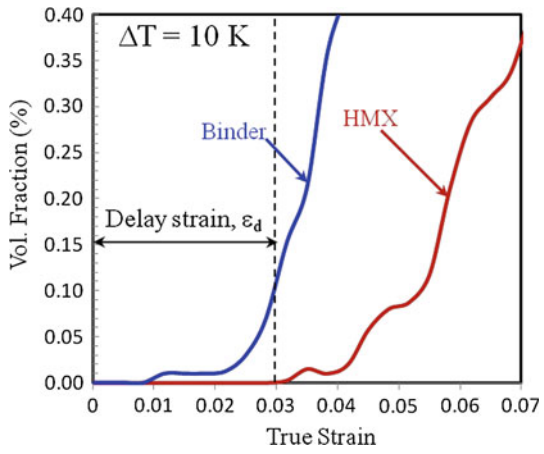

Fig. 8 Volume fractions of HMX grains and binder having a temperature rise of at least 10 K ($T_i = 300\,K$ and $\dot{\varepsilon} = 16,667\,s^{-1}$)

$$W_{ve}(t) = C(T_i) \cdot t; \quad t \geq 0. \tag{6.2}$$

In contrast to viscoelastic dissipation, frictional dissipation does not initiate until a delay strain (ε_d) or delay time (t_d) has elapsed. Once frictional dissipation (W_f) initiates, its rate (W'_f) varies linearly with time. Thus, the variation of frictional dissipation rate W'_f can be expressed as,

$$W'_f(t) = \begin{cases} 0; & 0 \leq t \leq t_d \\ D(T_i) \cdot t; & t \geq t_d, \end{cases} \tag{6.3}$$

where $D(T_i) = -71.9816 \cdot T_i(kW)$. The variation of frictional dissipation with time is, therefore,

$$W_f(t) = \begin{cases} 0; & 0 \leq t \leq t_d \\ D(T_i) \cdot (t - t_d)^2; & t \geq t_d. \end{cases} \tag{6.4}$$

Equations (6.3) and (6.4) are plotted in Figs. 8d–e. The fit for frictional dissipation agrees well with the calculated curves in Fig. 8c. A comparison of and W_{ve} and W_f shows that the onset of frictional dissipation has no appreciable impact on viscoelastic dissipation. Since W_{ve} has a linear dependence on tiem and W_f is a quadractic function of time, the onset of frictional dissipation signifies a transition in heating mechanism from one dominated by viscoelasticity to one dominated by internal friction. Figure 9 shows the volume fractions of binder and HMX granules having temperature rises of at least 10 K for the case with $T_i = 300\,K$. Heating in the HMX phase initiates at a nominal strain of 0.03 which is identical to the delay strain obtained earlier. Clearly, heating in the grains is primarily due to frictional dissipation which dominates the overall heating process once it sets in.

It can be inferred from Fig. 8c that the delay strain is not dependent on initial temperature and frictional dissipation initiates at the same level of overall strain. Previous experimental study by Govier et al. [5] showed that the failure strain or strain corresponding to peak stress of the PBX is invariant with respect to initial temperatures between 218 and 328 K. The experimental result and the results obtained here show that the initiation of fracture and friction in this PBX is not sensitive to initial temperature. On the other hand, packing density and loading rate are expected to play a more important role in affecting damage initiation consequently the delay strain.

The temperature rises in the binder and grains are quantified separately in Fig. 9. The histograms show the percentage by volume of each phase having a certain value of temperature increase after 5.0 μs of deformation at a strain rate of $\varepsilon = 16,667\,s^{-1}$. The strain ($\varepsilon = 7.5\,\%$) is identical for all four cases while the temperature rise is relative to the initial temperature. For all cases, most of the microstructure experiences lower temperature rises (∼5 K) and only smaller fractions of the volume experience higher values of ΔT. At both 210–300 K, significant heating takes place in the binder and grains, with the binder being heated more than the grains. More severe heating occurs in the binder at $T_i = 300\,K$, particularly at the low temperature end (∼5–10 K). Temperature increases at the lower end are primarily due to viscous dissipation in the binder which is partly conducted to the grains.

At $T_i = 210\,K$, temperature rises in the grains are almost twice that at $T_i = 300\,K$. This can be attributed to earlier fracture and higher frictional dissipation at lower initial temperatures. Thus, as the initial temperature is increased, viscous deformation of the binder delays the onset of grain-binder interfacial failure and more importantly, grain-grain interactions.

7 Concluding remarks

A fully coupled thermomechanical finite-deformation framework is used to analyze the response of polymer-bonded explosives (PBXs). The analyses carried out focus on composites consisting of HMX granules bonded by an estane matrix under conditions of deformation. Digitized micrograph of an actual PBX specimen is used in this analysis.

Initial temperatures between 210 and 300 K are considered, spanning across the glass transition temperature 243 K of the binder. A transition in failure mode from brittle fracture at temperatures below T_g to shear band formation at temperatures above T_g is observed. At the same level of overall deformation, more severe temperature rises are observed for lower initial temperatures due to more brittle responses of the binder, earlier fracture of the constituents, and more significant frictional heating at crack surfaces.

The energy dissipations contributing to temperature rises in the microstructure are quantified. In the process, a concept of delay strain is introduced which marks the transition in heating mechanism from viscoelastic to frictional

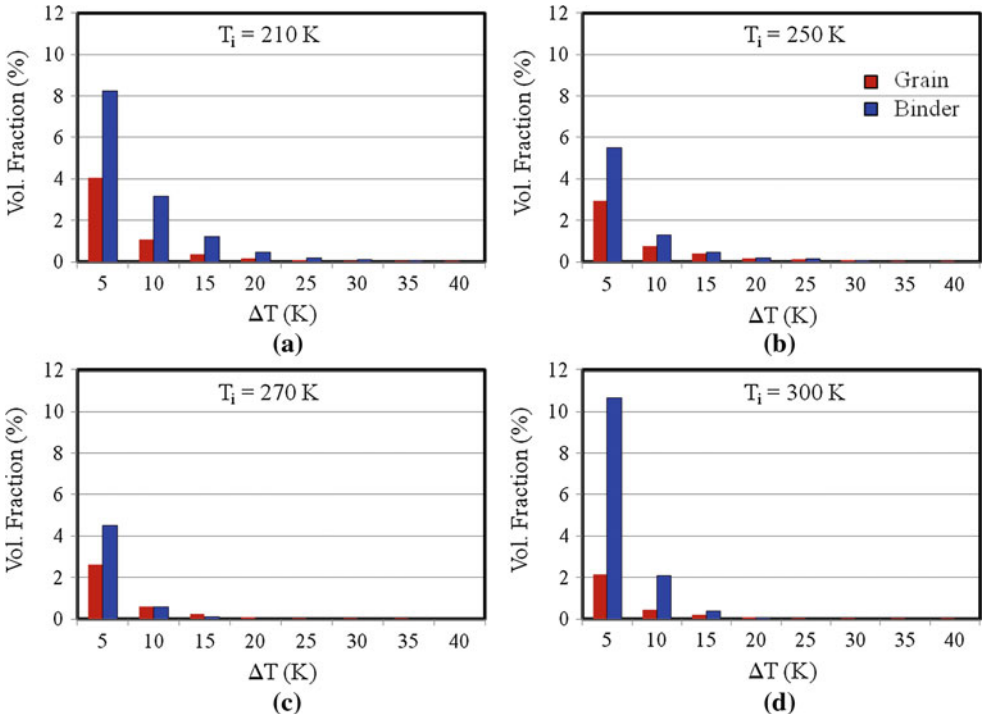

Fig. 9 Histograms showing fractions of binder and grains in terms of volume at different temperature ranges for $T_i = 210$–$300\,K$, $\dot{\varepsilon} = 16{,}667\,s^{-1}$, at $t = 5.0\ \mu m$ ($\varepsilon = 7.5\,\%$)

dissipation. The delay strain is found to be invariant with initial temperature. The framework developed and the results obtained are useful for establishing microstructure-performance relations for PBXs.

Acknowledgments The authors acknowledge support from the Air Force Research Laboratory (AFRL) at the Eglin AFB in Florida (scientific officers: Drs. Yasuyuki Horie and Jennifer Jordan) and the Defense Threat Reduction Agency (DTRA) (scientific officer: Dr. Suhithi Peiris). We are grateful to Dr. Horie for many helpful discussions. Calculations are carried out on parallel computers at NAVO and the DPRL at Georgia Institute of Technology.

References

1. Benson DJ, Conley P (1999) Eulerian finite-element simulations of experimentally acquired HMX microstructures. Model Simul Mater Sci Eng 7:333–354
2. Tarver CM, Chidester SK, Nichols AL (1996) Critical conditions for impact- and shock-induced hot spots in solid explosives. J Phys Chem 100:5794–5799
3. Tarver CM, Tran TD (2004) Thermal decomposition models for HMX-based plastic bonded explosives. Combust Flame 137:50–62
4. Gray GT III, Bluementhal WR, Idar DJ, Cady CM (1998) Influence of temperature on the high strain-rate mechanical behavior of PBX 9501. Schmidt SC, Dandekar DP, Forbes JW (eds) Shock compression of condensed matter, 1997, AIP press, Woodbury, pp 583–586
5. Govier RK, Gray GT, Blumenthal WR (2008) Comparison of the influence of temperature on the high-strain-rate mechanical responses of PBX 9501 and EDC37, pp 535–538
6. Blumenthal WR, Gray GT, Idar DJ, Holmes MD, Scott PD, Cady CM, Cannon DD (2000) Influence of temperature and strain rate on the mechanical behavior of PBX 9502 and Kel-F 800^{TM}. AIP Conf Proc 505:671
7. Tan H, Liu C, Huang Y, Geubelle PH (2005) The cohesive law for the particle/matrix interfaces in high explosives. J Mech Phys Solids 53:1892–1917
8. Baer MR (2002) Modeling heterogeneous energetic materials at the mesoscale. Thermochim Acta 384:351–367
9. Trott WM, Baer MR, Castaneda JN, Chhabildas LC, Asay JR (2007) Investigation of the mesoscopic scale response of low-density pressings of granular sugar under impact. J Appl Phys, 101(2):024917
10. Menikoff R (2003) Pore collapse and hot spots in HMX. Presented at the APS Topical Conference, Portland
11. Idar DJ, Straight JW, Osborn MA, Skidmore CB, Phillips DS, Buntain GA (2000) PBX 9501 high explosive violent reaction: phase II baseline and aged experiments. See http://www.fas.org/sgp/othergov/doe/lanl/lib-www/la-pubs/00538217.pdf.
12. Ortiz M, Pandolfi A (1999) Finite-deformation irreversible cohesive elements for three-dimensional crack-propagation analysis. Int J Numer Methods Eng 44:1267–1282
13. Banerjee B, Cady CM, Adams DO (2003) Micromechanics simulations of glass-estane mock polymer bonded explosives. Model Simul Mater Sci Eng 11:457–475
14. Wu Y-Q, Huang F-L (2009) A micromechanical model for predicting combined damage of particles and interface debonding in PBX explosives. Mech Mater 41:27–47
15. Barua A, Zhou M (2011) A Lagrangian framework for analyzing microstructural level response of polymer-bonded explosives. Model Simul Mater Sci Eng 19:24
16. Barua A, Horie Y, Zhou M (2012) Energy localization in HMX-Estane polymer-bonded explosives during impact loading. J Appl Phys 111:11

17. Barua A, Horie Y, Zhou M (2012) Microstructural level response of HMX-Estane polymer-bonded explosive under effects of transient stress waves. Proc Royal Soc 468:3725–3744
18. Barua A, Kim S, Horie Y, Zhou M (2012) Ignition criterion for heterogeneous energetic materials based on hotspot size-temperature threshold. J Appl Phys, (Under Peer Review)
19. Zhai J, Zhou M (2000) Finite element analysis of micromechanical failure modes in a heterogeneous ceramic material system. Int J Fract 101:161–180
20. Siviour CR, Laity PR, Proud WG, Field JE, Porter D, Church PD, Gould P, Huntingdon-Thresher W (2008) High strain rate properties of a polymer-bonded sugar: their dependence on applied and internal constraints. Proc Royal Soc Math Phys Eng Sci 464:1229–1255
21. Zhai J, Tomar V, Zhou M (2004) Micromechanical simulation of dynamic fracture using the cohesive finite element method. J Eng Mater Technol Trans ASME 126:179–191
22. Tomar V, Zhai J, Zhou M (2004) Bounds for element size in a variable stiffness cohesive finite element model. Int J Numer Methods Eng 61:1894–1920
23. Tvergaard V, Hutchinson JW (1992) The relation between crack-growth resistance and fracture process parameters in elastic plastic solids. J Mech Phys Solids 40:1377–1397
24. Camacho GT, Ortiz M (1996) Computational modelling of impact damage in brittle materials. Int J Solids Struct 33:2899–2938
25. Cady CM, Blumenthal WR, Gray GT, Idar DJ (2006) Mechanical properties of plastic-bonded explosive binder materials as a function of strain-rate and temperature. Polym Eng Sci 46:812–819
26. Rae PJ, Goldrein HT, Palmer SJP, Field JE, Lewis AL (2002) Quasi-static studies of the deformation and failure of beta-HMX based polymer bonded explosives. Proc Royal Soc Lond Ser A 458:743–762
27. Menikoff R, Sewell TD (2001) Constituent properties of HMX needed for meso-scale simulaitons. Los Alamos National Lab, Los Alamos